Letter

Transition from alternating stripes to alternating labyrinths in oscillatory media

Chunli Huang,[1] Zhen Song,[2] and Zhilin Qu[3,*]

[1]*School of Mathematics and Statistics, Guangdong University of Foreign Studies, Guangzhou 510420, China*

[2]*Pengcheng Laboratory, Shenzhen, Guangdong 518000, China*

[3]*Department of Medicine, University of California, Los Angeles, California 90095, USA*

(Received 5 December 2024; accepted 24 February 2025; published 13 March 2025)

Alternating (temporally period-2) stripes and labyrinths have been observed in media of chemical and biochemical reactions; however, the mechanisms underlying the formation of these spatiotemporal patterns remain unclear. Here, we conduct computer simulation using a modified model of Belousov−Zhabotinsky reaction that incorporates a global feedback loop with a spatial strength profile of Gaussian distribution. The simulation results demonstrate that the transition from alternating stripes to alternating labyrinths occurs when the feedback is negative with a certain width of the Gaussian function. We add the same Gaussian-weighted feedback loop to an amplitude equation to describe the amplitude dynamics of the period-2 oscillation and show that the pattern dynamics of the Belousov−Zhabotinsky reaction can be well captured by this amplitude equation. Analyses of the amplitude equation demonstrate that the transition from stripes to labyrinths arises from the transverse instabilities of bistable fronts caused by the Gaussian-weighted negative global feedback.

DOI: 10.1103/PhysRevE.111.L032201

Pattern formation is a fundamental process in natural and engineered systems [1,2]. In chemical and biological systems, steady-state patterns including stripes, spots, and labyrinths are widely observed, and Turing instability is known as a major underlying mechanism [3–6]. In oscillatory media, oscillatory patterns or more complex spatiotemporal patterns have been widely demonstrated [6–8]. One type of oscillatory pattern is oscillatory clusters or clustered standing waves observed in chemical reactions [9–14]. These oscillatory clusters exhibit temporally period-2 and spatially antiphase in neighboring regions, such as alternating stripes in two-dimensional (2D) media [Fig. 1(a)] [12]. Examples of this type of alternating patterns in biological systems are spatially discordant calcium alternans in cardiac myocytes and spatially discordant action potential duration alternans in cardiac tissue [15–18], both of which can cause lethal arrhythmias [19,20], and pole-to-pole oscillations of the Min proteins to ensure fidelity of cell division in Escherichia coli (E. coli) [21–24]. In addition to alternating stripes, alternating labyrinths [Fig. 1(b)] have also been observed in Belousov−Zhabotinsky (BZ) reactions [6,8,25] and in an *in vitro* E. coli system [26]. The alternating stripes [Fig. 1(a)] observed in chemical reaction experiments are caused by a uniform global feedback loop added externally to the experimental systems [10–12], which is also demonstrated in computer simulations of reaction-diffusion models with global feedback [10,12–14] or global coupling [9]. However, in either the chemical reaction experiments [10–12] or the computer models [9,10,12–14], no alternating labyrinths were observed, indicating that although the uniform global feedback loop can give rise to alternating stripes and clusters, a new mechanism for the occurrence of the labyrinths must exist. Furthermore, no computer models have been developed to unravel the mechanism for the formation of the alternating labyrinths. In this letter, we first carry out computer simulation of a modified BZ reaction model to demonstrate the transitions from alternating stripes to labyrinths. We then employ an amplitude equation approach to perform analytical treatments to reveal the underlying mechanisms.

The BZ reaction model with uniform global feedback was used previously to simulate alternating stripes [10,13]. Here, we add to this model a nonuniform global feedback loop with the feedback strength described by a Gaussian-weighted spatial average of a reactant. The partial differential equations of the modified BZ reaction are as follows:

$$\frac{\partial X}{\partial t} = \frac{-k_2X + k_3A}{k_2X + k_3A}\left[\frac{qk_7k_8BZ}{k_8 + k_{-7}h_0(C-Z)} + k_9B + \gamma(\bar{Z} - Z_t) + \varepsilon(\bar{Z}_g - Z_t)\right] - 2k_4X^2 + k_5h_0AX - k_{-5}U^2 + D_X\nabla^2X \tag{1}$$

$$\frac{\partial Z}{\partial t} = k_6U(C-Z) - k_{-6}XZ - \frac{k_7k_8BZ}{k_8 + k_{-7}h_0(C-Z)} + D_Z\nabla^2Z \tag{2}$$

where X and Z are the reactants, and U is a function of X and Z. $\gamma(\bar{Z} - Z_t)$ is the uniform global feedback term with $\bar{Z}$ being the spatial average of Z and $Z_t = 0.0005$. $\varepsilon(\bar{Z}_g - Z_t)$ is the nonuniform global feedback term with $\bar{Z}_g$ a Gaussian-weighted spatial average of Z, i.e.,

$$\bar{Z}_g(x,y,t) = \frac{1}{N2\pi\sigma^2}\iint_{-\frac{L}{2}-x,\ -\frac{L}{2}-y}^{\frac{L}{2}-x,\ \frac{L}{2}-y} Z(x',y',t) \times e^{-[(x'-x)^2+(y'-y)^2]/2\sigma^2}dx'dy' \tag{3}$$

*Contact author: zqu@mednet.ucla.edu

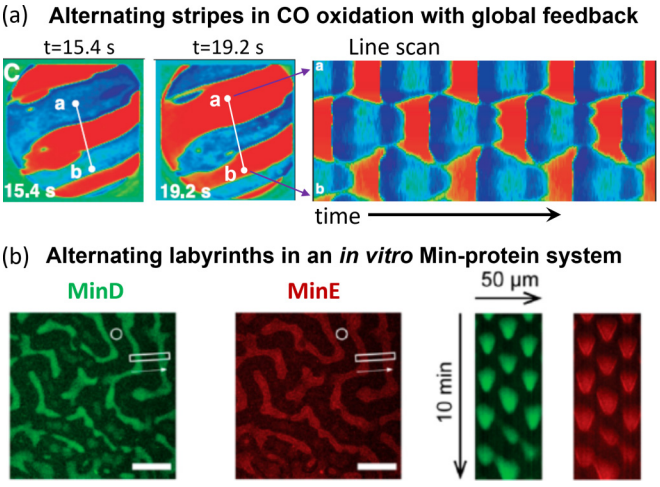

FIG. 1. Alternating stripes and labyrinths in experimental systems. (a) Alternating stripes in catalytic CO oxidation on a platinum surface, adapted from Kim *et al.* [12]. The left two panels are snapshots of opposite phases (at 15.4 s and 19.2 s) and the right panel is a line scan (space-time plot) from the marked line (from a to b). (b) Alternating labyrinths of bacterial proteins in an *in vitro* system of MinD and MinE, adapted from Kretschmer *et al.* [26]. The left two panels are snapshots of MinD and MinE. The right two panels are line scans from the corresponding regions marked by the open bars on the left panels.

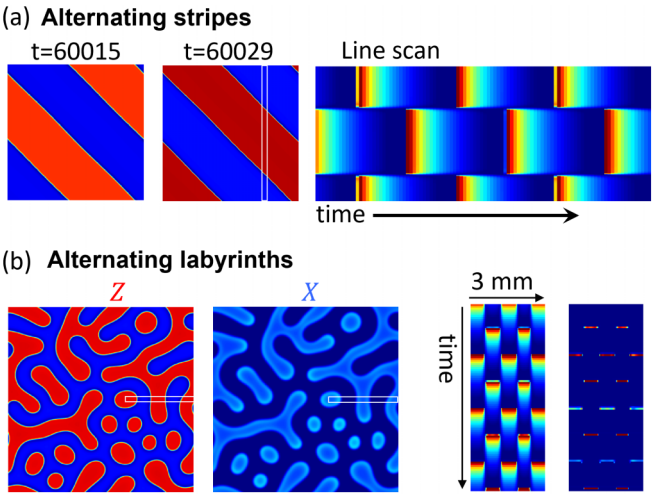

FIG. 2. Alternating patterns in a 2D model of BZ reaction. (a) Alternating stripes. $\sigma = 4$ mm. Left: Snapshots of reactant Z taken at two time points of opposite phases. Right: Line scan from a vertical line marked by the open bar. (b) Alternating labyrinths. $\sigma = 0.24$ mm. Left two panels: Snapshots of reactants Z and X. Right two panels: Line scans of the two reactants from the open bars marked in the left panels. Medium size is $8 \times 8\,\mathrm{mm}^2$.

In Eq. (3), N is the normalization constant, x and y are the spatial coordinates, and L is the dimension of the 2D medium. A periodic boundary condition is used. The parameters are the same as in Refs. [10,13] except that we set $\gamma = 1$ and $\varepsilon = -0.01$. We vary σ to generate different patterns. The rationale for using the Gaussian-weighted feedback term is that in chemical or biochemical reactions, reactants diffuse in space, and thus the feedback loops are neither localized nor uniformly global but in-between. A Gaussian distribution is a proper description of the diffusion process, and the width (σ) of the Gaussian function represents the diffusion speed. The feedback is completely local when $\sigma = 0$ and uniformly global when $\sigma \to \infty$. In numerical simulations, the differential equations are discretized with $\Delta x = \Delta y = 0.02$ mm and $\Delta t = 0.001$ s. Computer simulations show that when σ is large (including $\sigma \to \infty$, i.e., the uniform global feedback), only alternating stripes are observed [Fig. 2(a)], but when σ is in the intermediate range, alternating labyrinths [Fig. 2(b)] are observed, which are similar to those observed in experiments [Fig. 1(b)]. In other words, this new BZ reaction model shows that a transition from alternating stripes to alternating labyrinths occurs when the global feedback changes from uniform to nonuniform, or when the width (σ) of the Gaussian function reduces to a certain value.

Owing to the complexity of the BZ reaction model, analytical treatments to reveal the underlying mechanism of the transition become nontrivial. To perform stability or bifurcation analyses for mechanistic understanding, we employ an amplitude equation approach that allows us to perform theoretical analyses. We previously used amplitude equation to investigate the spatiotemporal dynamics of cardiac alternans [27,28], and here we modify the amplitude equation by adding a Gaussian-weighted global feedback term, i.e.,

$$\frac{\partial a}{\partial t} = \alpha a - \beta a^3 + \nabla^2 a + \varepsilon \bar{a}_g \tag{4}$$

where a is the amplitude of alternating (period-2) state, and $\bar{a}_g$ is the Gaussian-weighted spatial average of a defined the same way as in Eq. (3) (replacing Z with a in Eq. (3)). In numerical simulations, Eq. (4) is discretized with $\Delta x = \Delta y = 1$ and $\Delta t = 0.01$, and we set $\alpha = 0.5$, $\beta = 0.0001$, and $\varepsilon = -0.1$ as default parameters unless stated explicitly. A periodic boundary condition is used. An amplitude equation was first derived by Echebarria and Karma [29] to describe the dynamics of spatially discordant action potential duration alternans during cardiac conduction in a one-dimensional (1D) cable. Their amplitude equation is simply Eq. (4) plus a convection term accounting for conduction but without the feedback term. a in Eq. (4) is defined as [left panel in Fig. 3(a)]: $a_n = (-1)^n(A_n - A_{n-1})/2$. In cardiac systems, A_n is either action potential duration or calcium amplitude [15,27–30], here it can be considered as the amplitude of X or Z in the BZ reaction. Assuming $t = nT$ as a continuous variable, one converts the discretized time series a_n to a continuous time series $a(t)$. With these operations, one transforms an alternating pattern into a stable steady-state pattern [right two panels in Fig. 3(a)] and obtains the amplitude equation [29]. With the presence of the Gaussian-weighted feedback, Eq. (4) can exhibit interesting pattern dynamics, such as the transition from stripes to labyrinths.

Using numerical simulations of Eq. (4), we find that for a given ε, labyrinths occur when σ is in the intermediate range [Fig. 3(b)]. When σ is either large or small, we do not observe labyrinths but stripes. These patterning behaviors are the same as those in the BZ reaction model [Fig. 3(c)], indicating that Eq. (4) can well capture the pattern dynamics of the modified

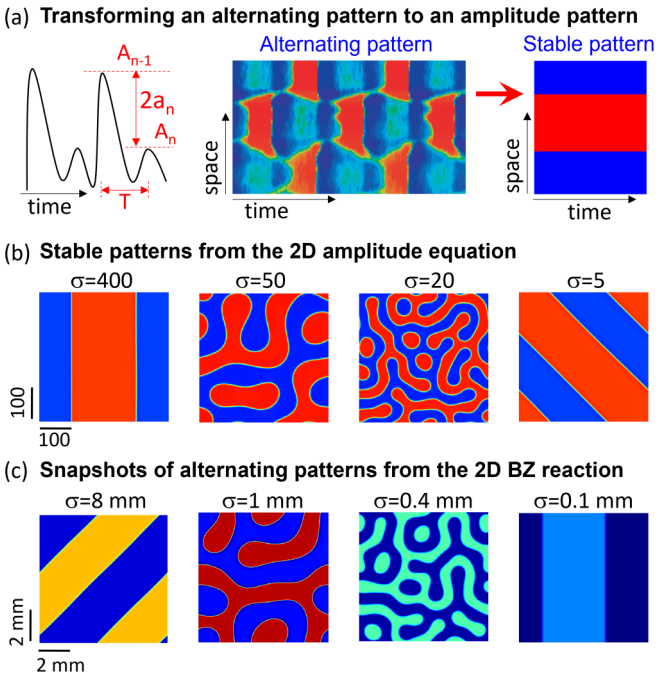

FIG. 3. Pattern dynamics in the amplitude equation and the BZ reaction-diffusion model. (a) Left panel: Schematic plot defining the amplitude of a period-2 (alternating) state. A_n is the peak value of the n^{th} cycle, and a_n is defined as the amplitude of the alternating state. T is the period. Right two panels: Schematic plots showing the conversion of an alternating pattern to a stable amplitude pattern. (b) Stable patterns from the amplitude equation for different σ. (c) Snapshots of $Z(x, y)$ from the oscillating BZ reaction for different σ taken at the end of each simulation. Parameters are the same as in Fig. 2(b).

BZ reaction model in the alternating (temporally period-2) regime.

Compared to the BZ reaction model Eqs. (1)–(3), the advantage of the amplitude equation Eq. (4) is that in addition to being computationally much easier, one can perform stability analyses to understand the mechanisms of alternating pattern formation, particularly the transition from alternating stripes to alternating labyrinths. We first analyze the stability of the uniform steady-state solutions and then the nonuniform steady-state (front) solutions.

For a uniform state, the feedback term in Eq. (4) becomes trivial, i.e., $\bar{a}_g = a$, and thus Eq. (4) exhibits the following uniform steady-state solutions: $a_s = 0$ and $a_s = \pm\sqrt{(\alpha+\varepsilon)/\beta}$. For simplicity, we first consider the stability of the uniform steady-state solutions in a 1D medium. For a 1D medium, the Gaussian feedback term has the following form: $\bar{a}_g(x,t) = \frac{1}{N\sqrt{2\pi}\sigma}\int_{-\frac{L}{2}-x}^{\frac{L}{2}-x} a(x',t)e^{-(x'-x)^2/2\sigma^2}dx'$. Linearizing Eq. (4) around the steady-state solution, i.e., expressing $a(x,t) = a_s + \xi e^{\lambda t+ikx}$ with ξ being the amplitude of the small perturbation, the Gaussian feedback term then becomes:

$$\bar{a}_g(x,t) = \frac{1}{N\sqrt{2\pi}\sigma}\int_{-\frac{L}{2}-x}^{\frac{L}{2}-x}(a_s + \xi e^{\lambda t+ikx'})e^{-(x'-x)^2/2\sigma^2}dx' \tag{5}$$

For an arbitrary size L, the integral in Eq. (5) cannot be explicitly solved. When the 1D medium is infinitely large, i.e., $L \to \infty$ (or practically $L \gg \sigma$), Eq. (5) can be explicitly solved, giving rise to $\bar{a}_g(x,t) = a_s + \xi e^{-\frac{\sigma^2k^2}{2}}e^{\lambda t+ikx}$. Inserting the linearized $a(x,t)$ and $\bar{a}_g(x,t)$ into Eq. (4), one obtains the eigenvalue λ as a function of wave number k for the zero steady-state solution ($a_s = 0$) as

$$\lambda_k = \alpha - k^2 + \varepsilon e^{-\frac{\sigma^2k^2}{2}} \tag{6}$$

When $\varepsilon = 0$, there are always unstable modes when $\alpha > 0$ since λ_k decreases with k monotonically. When $\varepsilon < 0$, λ_k becomes a nonmonotonic function of k [Fig. 4(a)]. From Eq. (6), one obtains the k value at the maximum of λ_k, i.e., $k_{\max} = \sqrt{\frac{-2}{\sigma^2}ln\frac{-2}{\varepsilon\sigma^2}}$. Inserting $k = k_{\max}$ into Eq. (6) and setting $\lambda_k = 0$, one obtains the stability boundary as $\alpha = \frac{2}{\sigma^2}(1-ln\frac{-2}{\varepsilon\sigma^2})$ or $\varepsilon = \frac{-2}{\sigma^2}e^{(\frac{\alpha\sigma^2}{2}-1)}$. We plot this boundary for $\alpha = 0.5$ in Fig. 4(b) (the green curve). The zero steady-state solution is unstable above this boundary. Once this steady state is unstable, nonuniform solutions emerge in the system [27,28]. In other words, nonuniform solutions exist above the green curve. Note that in this symmetric bistable system, a nonuniform solution is just a front solution with zero speed (see below).

Following the same approach, for the nonzero uniform steady-state solutions ($a_s = \pm\sqrt{(\alpha+\varepsilon)/\beta}$), the eigenvalue is

$$\lambda_k = -2\alpha - 3\varepsilon - k^2 + \varepsilon e^{-\frac{\sigma^2k^2}{2}} \tag{7}$$

Similar to the case of the zero steady-state solution, by inserting $k = k_{\max}$ into Eq. (7) and setting $\lambda_k = 0$, one obtains the stability boundary as: $\alpha = -\frac{3}{2}\varepsilon - \frac{1}{\sigma^2}(1-ln\frac{-2}{\varepsilon\sigma^2})$. We plot this boundary for $\alpha = 0.5$ in Fig. 4(b) (the red curve). The nonzero uniform steady-state solutions are unstable below this boundary.

For the stability of the uniform steady-state solutions in a 2D medium, one simply replaces k^2 by $k_x^2 + k_y^2$ in Eqs. (6) and (7) to take into account the Fourier modes in both directions. However, the stability boundaries are the same as predicted by Eq. (6) or Eq. (7) for the 1D medium.

Therefore, from this simple stability analysis, one can predict that nonuniform solutions exist above the green curve in Fig. 4(b) since the uniform steady-state solution $a_s = 0$ is unstable. Above the red curve, nonuniform solutions and the uniform steady-state solution coexist since the uniform steady-state solution $a_s = \pm\sqrt{(\alpha+\varepsilon)/\beta}$ is stable in this region. Note that in the case of Fig. 3(b), since $\varepsilon = -0.1$ is above the red curve and thus the uniform pattern is stable for all σ. We did not show the uniform patterns in Fig. 3(b). The region right to the green curve and below the red curve only exhibits nonuniform solutions since both the zero and nonzero uniform steady-state solutions are unstable.

Now the question is whether the nonuniform (front) solutions (stripes) in a 2D medium are stable or not. Due to the presence of the feedback term, nonuniform solutions cannot be obtained analytically, unless under certain limits. For example, when $\sigma \to \infty$, the Gaussian function approaches zero and then $\bar{a}_g = 0$. Under this condition, a front solution can be obtained (for $L \to \infty$ and open boundary condition) as [2,27,28,31]: $a_s(x) = \sqrt{\frac{\alpha}{\beta}}\tanh(\sqrt{\frac{\alpha}{2}}x)$. When $\sigma \to 0$, one

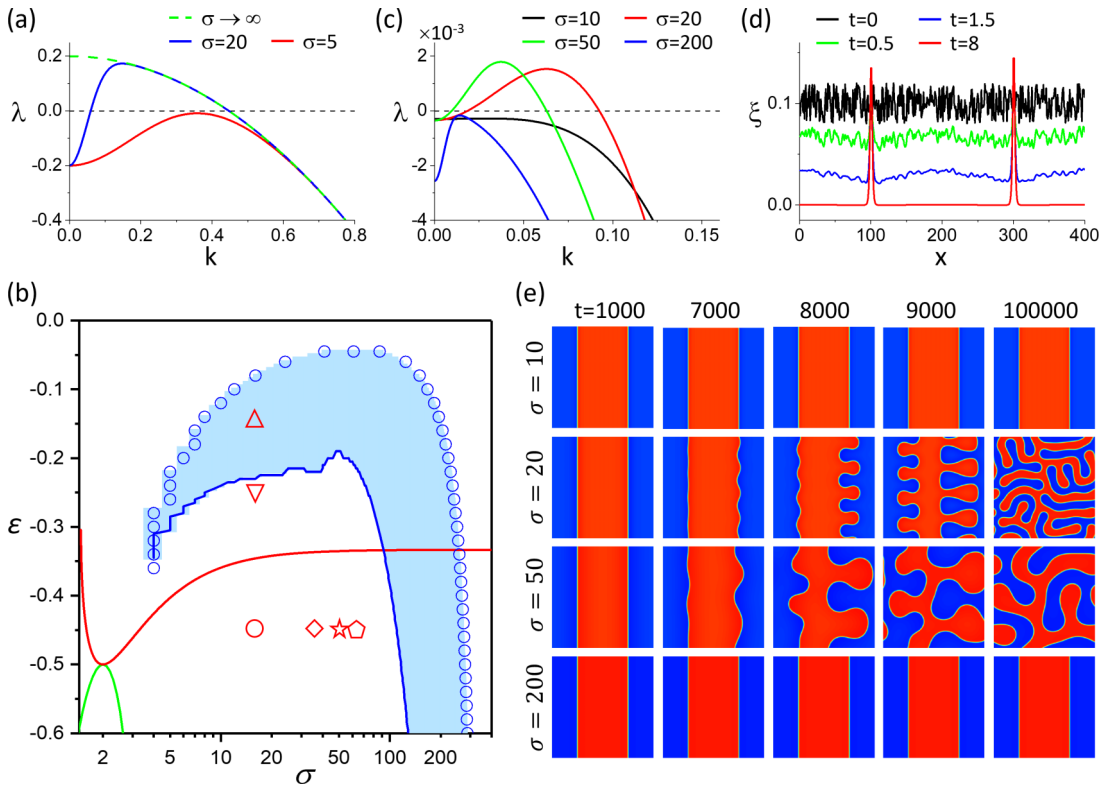

FIG. 4. Front instability in 2D media. (a) λ versus k for the zero steady-state solution (Eq. (6)) for different σ as marked. $\alpha = 0.2$ and $\varepsilon = -0.4$. (b) Stability boundaries in σ-ε plane. Green line is the stability boundary for $a_s = 0$ and red line for $a_s = \pm\sqrt{(\alpha+\varepsilon)/\beta}$. The cyan region is where the single-stripe front solutions are transversely unstable. The upper boundary was determined by calculating the Lyapunov exponent using Eq. (9). Blue circles on the upper boundary mark the boundary determined from direct 2D simulations [examples shown in (e)]. The lower boundary was determined (blue line) by the stability of the single-stripe solutions in the 1D medium using Eq. (4), or the single-stripe solutions are longitudinally unstable below the blue line. (c) λ vs k calculated using Eq. (9) for the single-stripe front solution for different σ values. (d) $\xi(x,t)$ at different time points for the case of $\sigma = 50$. (e) Snapshots of a in a 400×400 medium at different time points and σ values as marked. The initial condition (t = 0) is a single-stripe front solution (pattern in the first column). A small random perturbation is given at $t = 1000$.

can treat the Gaussian function as a δ-function and then $\bar{a}_g = a$. Under this condition, a front solution can be obtained as: $a_s(x) = \sqrt{\frac{\alpha+\varepsilon}{\beta}}\tanh(\sqrt{\frac{\alpha+\varepsilon}{2}}x)$. Nonetheless, we obtain $a_s(x)$ numerically using the 1D medium for a given σ. Without the feedback term in Eq. (4), the stability of the front solutions is neutral. As shown in our previous studies [28,30], a negative global feedback loop can stabilize the front solutions.

To investigate the stability of a front solution (stripes) in a 2D medium, we add a perturbation to the solution as follows:

$$a(x, y, t) = a_s(x) + \xi(x, t)e^{iky} \tag{8}$$

Inserting Eq. (8) into Eq. (4), one obtains the following equation for $\xi(x,t)$:

$$\frac{\partial \xi(x,t)}{\partial t} = \{\alpha - 3\beta[a_s(x)]^2\}\xi(x,t) + \frac{\partial^2 \xi(x,t)}{\partial x^2} - k^2\xi(x,t) + \varepsilon e^{\frac{-\sigma^2 k^2}{2}} \int_{-\frac{L}{2}-x}^{\frac{L}{2}-x} \frac{\xi(x',t)}{N\sqrt{2\pi}\sigma} e^{-(x'-x)^2/2\sigma^2} dx' \tag{9}$$

Once $a_s(x)$ is determined, we examine its stability by calculating the maximum Lyapunov exponent using the formula: $\lambda = \lim_{t\to\infty} \frac{1}{t} ln \frac{\|\xi(x,t)\|}{\|\xi(x,0)\|}$ with $\xi(x,t)$ numerically solved using Eq. (9). For a given k, one can obtain a λ, and thus obtain the curve of λ versus k. Figure 4(c) shows λ versus k for different σ values for a single-stripe solution [see the pattern in the first column in Fig. 4(e)], which is a double-front solution under periodic boundary condition. For both small and large σ, $\lambda < 0$ for any k, indicating that the stripe is stable in the 2D medium [also see the 2D examples ($\sigma = 10$ and $\sigma = 200$) in Fig. 4(e)]. For intermediate σ, λ can be positive for certain k values, indicating that the stripe is unstable in the 2D medium [also see the 2D examples ($\sigma = 20$ and $\sigma = 50$) in Fig. 4(e)]. Fig. 4(d) shows $\xi(x,t)$ at 4 time points for the case of $\sigma = 50$ for which the stripe is unstable. $\xi(x)$ grows at the front regions but shrinks at other regions, indicating that the transverse instabilities occur at the front regions.

To investigate how the transverse instability is affected by the Gaussian-weighted feedback, we scan σ and ε to determine the stability boundary of the single-stripe front solution by calculating λ using Eq. (9). The stripe pattern is unstable in the colored region and labyrinths emerge. The upper boundary of the colored region is where transverse instability occurs. The lower boundary is where the single-stripe solution is unstable in the 1D medium (longitudinal instability, not the transverse instability as for the upper boundary). To confirm the theoretical predictions, we also carry out 2D simulations by adding a random perturbation to the single-stripe front

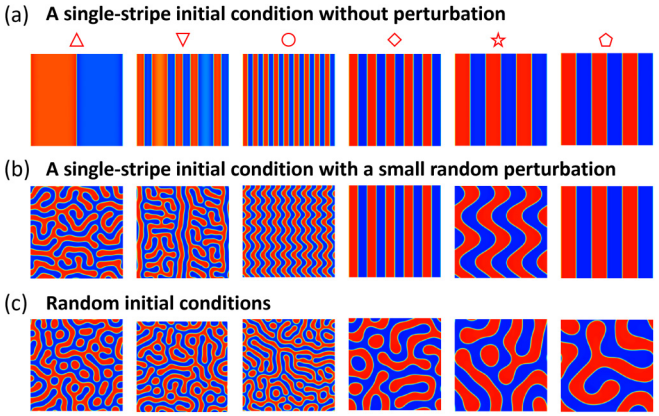

FIG. 5. Initial condition dependent patterns. (a) Steady-state patterns (taken at $t = 10000$) started from a single-stripe pattern (as the pattern in the first panel) at the parameter locations indicated by the symbols marked on Fig. 4(b). (b) Same as (a) but a random perturbation is given at $t = 1000$. (c) Steady-state patterns started from random initial conditions for the same parameters as in (a) and (b). The parameter sets (σ, ε) are (left to right): (15, –0.15), (15, –0.25), (15, –0.45), (35, –0.45), (50, –0.45), and (60, –0.45).

solution to examine the transverse instability [snapshots in Fig. 4(e) show the stabilities of the fronts for selected σ]. The blue circles in Fig. 4(b) mark the stability boundary determined by the direct 2D simulations, which agree accurately with the theoretical prediction using the Lyapunov exponent calculated from simulations of Eq. (9). Note that the colored region is determined solely by the stability of the single-stripe solution but there are multi-stripe solutions [27,30] with their own longitudinal and transverse instabilities. In general, the multi-stripe solutions are more stable than the single-stripe solution. Because of this, in the colored region in Fig. 4(b), multi-stripe patterns coexist with labyrinths. Below the colored region (or the blue curve), the single-stripe solution undergoes longitudinal instability, leading to multi-stripe steady-state patterns if no random perturbations are given [the panels from the downward triangle in Fig. 5(a)]. If a small random perturbation is given at some time point ($t = 1000$ in the simulations), it results in different patterns for different parameter locations [Fig. 5(b)]: labyrinths, wavy stripes, and straight stripes (the same as those without perturbation). This indicates that the multi-stripe patterns are either transversely unstable or stable, depending on the parameter locations. However, when started with random initial conditions, the resulting steady-state patterns are all labyrinths [Fig. 5(c)]. Theoretically, we can use Eq. (9) to perform stability analyses of the multi-stripe solutions to obtain a more complete phase diagram. However, the structure of the phase diagram on the σ-ε plane is too complex to elaborate in detail in this study. Our focus here is on the mechanism of transition from alternating stripes to labyrinths, and we will investigate the spatiotemporal alternating pattern dynamics in more detail using both the amplitude equation and the modified BZ reaction model in a future study.

In summary, alternating labyrinths are caused by a transverse instability of the front solutions. The instability is promoted by a negative global feedback loop with a Gaussian-weighted feedback strength function. This nonuniform negative global feedback corresponds to an inhibitor with a certain diffusion speed in a reaction-diffusion system, which is similar to the molecular conditions giving rise to Turing instability for pattern formation. Although models and theories have widely been developed for understanding stationary pattern formation and their transitions, our work in this study reveals the mechanism for transition from alternating stripes to alternating labyrinths and provides a theoretical means, particularly the modified amplitude equation, for investigating the dynamical mechanisms for the formation of alternating (temporally period-2) patterns widely observed in chemical [6,8,10–12,25], biochemical [21–24,26,32,33], and physiological [20] systems.

This study was supported by grants from National Institutes of Health (R01 HL175074 and P01 HL164311 to Z.Q.), Natural Science Foundation of China (No. 82172067 to Z.S.), and Major Key Project of Pengcheng Laboratory (PCL2023A09 to Z.S.).

[1] P. Ball, *The Self-Made Tapestry: Pattern Formation in Nature* (Oxford University Press, Oxford, 1999).
[2] M. Cross and H. Greenside, *Patern Formation and Dynamics in Nonequilibrium Systems* (Cambridge University Press, Cambridge, 2009).
[3] A. M. Turing, The chemical basis of morphogenesis, Phil. Roy. Soc. Lond. B **237**, 37 (1952).
[4] S. Kondo and T. Miura, Reaction-diffusion model as a framework for understanding biological pattern formation, Science **329**, 1616 (2010).
[5] P. K. Maini, R. E. Baker, and C. M. Chuong, The Turing model comes of molecular age, Science **314**, 1397 (2006).
[6] V. K. Vanag and I. R. Epstein, Pattern formation mechanisms in reaction-diffusion systems, Int. J. Dev. Biol. **53**, 673 (2009).
[7] V. Petrov, Q. Ouyang, and H. L. Swinney, Resonant pattern formation in a chemical system, Nature (London) **388**, 655 (1997).
[8] V. K. Vanag and I. R. Epstein, Pattern formation in a tunable medium: The Belousov-Zhabotinsky reaction in an aerosol OT microemulsion, Phys. Rev. Lett. **87**, 228301 (2001).
[9] M. Falcke, H. Engel, and M. Neufeld, Cluster formation, standing waves, and stripe patterns in oscillatory active media with local and global coupling, Phys. Rev. E **52**, 763 (1995).
[10] V. K. Vanag, L. Yang, M. Dolnik, A. M. Zhabotinsky, and I. R. Epstein, Oscillatory cluster patterns in a homogeneous chemical system with global feedback, Nature (London) **406**, 389 (2000).
[11] V. K. Vanag, A. M. Zhabotinsky, and I. R. Epstein, Pattern formation in the Belousov−Zhabotinsky reaction with photochemical global feedback, J. Phys. Chem. A **104**, 11566 (2000).
[12] M. Kim, M. Bertram, M. Pollmann, A. v. Oertzen, A. S. Mikhailov, H. H. Rotermund, and G. Ertl, Controlling chemical turbulence by global delayed feedback: Pattern formation in catalytic CO oxidation on Pt(110), Science **292**, 1357 (2001).

[13] L. Yang, M. Dolnik, A. M. Zhabotinsky, and I. R. Epstein, Oscillatory clusters in a model of the photosensitive Belousov-Zhabotinsky reaction system with global feedback, Phys. Rev. E **62**, 6414 (2000).

[14] M. Bertram and A. S. Mikhailov, Pattern formation in a surface chemical reaction with global delayed feedback, Phys. Rev. E **63**, 066102 (2001).

[15] Y. Shiferaw and A. Karma, Turing instability mediated by voltage and calcium diffusion in paced cardiac cells, Proc. Natl. Acad. Sci. USA. **103**, 5670 (2006).

[16] S. A. Gaeta, G. Bub, G. W. Abbott, and D. J. Christini, Dynamical mechanism for subcellular alternans in cardiac myocytes, Circ. Res. **105**, 335 (2009).

[17] J. M. Pastore, S. D. Girouard, K. R. Laurita, F. G. Akar, and D. S. Rosenbaum, Mechanism linking T-wave alternans to the genesis of cardiac fibrillation, Circulation **99**, 1385 (1999).

[18] Z. Qu, A. Garfinkel, P. S. Chen, and J. N. Weiss, Mechanisms of discordant alternans and induction of reentry in simulated cardiac tissue, Circulation **102**, 1664 (2000).

[19] W. Liu, T. Y. Kim, X. Huang, M. B. Liu, G. Koren, B. R. Choi, and Z. Qu, Mechanisms linking T-wave alternans to spontaneous initiation of ventricular arrhythmias in rabbit models of long QT syndrome, J. Physiol. **596**, 1341 (2018).

[20] Z. Qu and J. N. Weiss, Cardiac alternans: From bedside to bench and back, Circ. Res. **132**, 127 (2023).

[21] D. M. Raskin and P. A. J. de Boer, Rapid pole-to-pole oscillation of a protein required for directing division to the middle of Escherichia coli, Proc. Natl. Acad. Sci. USA. **96**, 4971 (1999).

[22] X. Fu, Y.-L. Shih, Y. Zhang, and L. I. Rothfield, The MinE ring required for proper placement of the division site is a mobile structure that changes its cellular location during the Escherichia coli division cycle, Proc. Natl. Acad. Sci. USA. **98**, 980 (2001).

[23] R. A. Kerr, H. Levine, T. J. Sejnowski, and W.-J. Rappel, Division accuracy in a stochastic model of Min oscillations in Escherichia coli, Proc. Natl. Acad. Sci. USA. **103**, 347 (2006).

[24] H. Meinhardt and P. A. J. de Boer, Pattern formation in Escherichia coli: A model for the pole-to-pole oscillations of Min proteins and the localization of the division site, Proc. Natl. Acad. Sci. USA. **98**, 14202 (2001).

[25] A. Kaminaga, V. K. Vanag, and I. R. Epstein, Wavelength halving in a transition between standing waves and traveling waves, Phys. Rev. Lett. **95**, 058302 (2005).

[26] S. Kretschmer, T. Heermann, A. Tassinari, P. Glock, and P. Schwille, Increasing MinD's membrane affinity yields standing wave oscillations and functional gradients on flat membranes, ACS Synth. Biol. **10**, 939 (2021).

[27] C. Huang, Z. Song, Z. Di, and Z. Qu, Stability of spatially discordant repolarization alternans in cardiac tissue, Chaos **30**, 123141 (2020).

[28] C. Huang, Z. Song, and Z. Qu, Synchronization of spatially discordant voltage and calcium alternans in cardiac tissue, Phys. Rev. E **106**, 024406 (2022).

[29] B. Echebarria and A. Karma, Instability and spatiotemporal dynamics of alternans in paced cardiac tissue, Phys. Rev. Lett. **88**, 208101 (2002).

[30] Z. Song and Z. Qu, Delayed global feedback in the genesis and stability of spatiotemporal excitation patterns in paced biological excitable media, PLoS Comput. Biol. **16**, e1007931 (2020).

[31] J. P. Keener and J. Sneyd, *Mathematical Physiology* (Springer, New York, 1998), p. 766.

[32] K. Zieske and P. Schwille, Reconstitution of self-organizing protein gradients as spatial cues in cell-free systems, eLife **3**, e03949 (2014).

[33] S. Kohyama, A. Merino-Salomón, and P. Schwille, In vitro assembly, positioning and contraction of a division ring in minimal cells, Nat. Commun. **13**, 6098 (2022).